

Examining Two-Dimensional Luminosity-time Correlations for Gamma Ray Burst Radio Afterglows with VLA and ALMA

DELINA LEVINE ¹, MARIA DAINOTTI ^{2,3,4}, KEVIN J. ZVONAREK ⁵, NISSIM FRAIJA ⁶, DONALD C. WARREN ⁷,
POONAM CHANDRA ⁸, AND NICOLE LLOYD-RONNING ^{9,10}

¹*Department of Astronomy, University of Maryland, College Park, MD 20742, USA*

²*National Astronomical Observatory of Japan, 2-21-1 Osawa, Mitaka, Tokyo 181-8588, Japan*

³*Space Science Institute, Boulder, CO, USA*

⁴*The Graduate University for Advanced Studies, SOKENDAI, Shonankokusaimura, Hayama, Miura District, Kanagawa 240-0193, Japan*

⁵*Department of Physics, University of Michigan, Ann Arbor, MI 48109, USA*

⁶*Instituto de Astronomía, Universidad Nacional Autónoma de México Circuito Exterior, C.U., A. Postal 70-264, 04510 México D.F., México*

⁷*RIKEN Interdisciplinary Theoretical and Mathematical Sciences Program (iTHEMS), Wakō, Saitama, 351-0198 Japan*

⁸*National Centre for Radio Astrophysics, Tata Institute of Fundamental Research, Ghaneshkhind Pune 411007, India*

⁹*Computational Physics and Methods Group (CCS-2), Los Alamos National Lab, Los Alamos, NM, USA 87545*

¹⁰*Department of Science and Engineering, University of New Mexico, Los Alamos, 87544*

(Accepted 18 November 2021)

Submitted to ApJ

ABSTRACT

Gamma-ray burst (GRB) afterglow emission can be observed from sub-TeV to radio wavelengths, though only 6.6% of observed GRBs present radio afterglows. We examine GRB radio light curves (LCs) to look for the presence of radio plateaus, resembling the plateaus observed in X-ray and optical. We analyze 404 GRBs from the literature with observed radio afterglow and fit 82 GRBs with at least 5 data points with a broken power law (BPL) model, requiring 4 parameters. From these, we find 18 GRBs that present a break feature resembling a plateau. We conduct the first multi-wavelength study of the Dainotti correlation between the luminosity L_a and the rest-frame time of break T_a^* for those 18 GRBs, concluding that the correlation exists and resembles the corresponding correlation in X-ray and optical wavelengths after correction for evolutionary effects. We compare the T_a^* for the radio sample with T_a^* values in X-ray and optical data (Dainotti et al. 2013, 2020b), finding significantly later break times in radio. We propose that this late break time and compatibility in slope suggests either a long-lasting plateau or the passage of a spectral break in the radio band. We also correct the distribution of the isotropic energy E_{iso} vs. the rest-frame burst duration T_{90}^* for evolutionary effects and conclude that there is no significant difference between the T_{90}^* distribution for the radio LCs with a break and those without.

1. INTRODUCTION

Gamma-ray bursts (GRBs) are observed in all wavelengths, from high energy gamma-rays to radio. GRBs are characterized by an energetic “prompt emission” of γ -rays followed by a much longer period of lower-energy emission called the “afterglow”, lasting from hundreds of seconds to years. X-ray, optical, and radio afterglows are not observed equally: X-ray afterglows have been detected in $\sim 66\%$ of observed GRBs when we consider the full sample of detected GRBs including the GRBs which are not only observed by the Neil Gehrels Swift Observatory (Swift), optical

Corresponding author: Maria Dainotti
maria.dainotti@nao.ac.jp

³ First and second authors contributed equally to this paper

arXiv:2111.10428v1 [astro-ph.HE] 19 Nov 2021

afterglows in 38%, and radio afterglows in only 6.6% of all known GRBs (Greiner 2021).¹ Indeed, some GRBs are too faint to be detected in radio (Chandra & Frail 2012). With the new Square Kilometer Array (SKA) facilities (Bij de Vaate et al. 2021) and SKA pathfinder (Johnston et al. 2007; Schinckel et al. 2011) we will be able to observe the radio afterglows of more GRBs. Out of the total number of GRBs observed in radio, we count that the majority (152) are observed by the Very Large Array (VLA).

Swift light curves (LCs) resulting from GRB afterglows have highlighted complicated features inconsistent with a simple power law decay (Sakamoto et al. 2007; Zhang et al. 2009). Analysis of X-ray LCs has shown the existence of plateaus, or a flattening in the afterglow emission between the prompt emission and the subsequent afterglow decay (Sakamoto et al. 2007; Dainotti et al. 2013; Fraija et al. 2020b,a). These plateaus have also been confirmed in optical LCs (Dainotti et al. 2020b).

An interesting two-dimensional correlation between the luminosity, L_a , and the rest-frame end time of the plateau, T_a^* , known as the Dainotti correlation, was discovered more than a decade ago (Dainotti et al. 2008, 2011a, 2013, 2015a, 2016, 2017b,a, 2020a,b; Srinivasaragavan et al. 2020) and has been proposed as a tool to standardize the plateau sample of GRBs. These plateaus are thought to be produced by continuous energy injection. One proposed explanation is accretion falling back onto a black hole, where energy is released into the external shock, interacting with the surrounding medium and injecting energy into the observed afterglow (Liang et al. 2007; Oates et al. 2012). Another interpretation involves the spin-down luminosity from a newborn magnetar providing the continuous energy injection (Thompson & Duncan 1993; Duncan & Thompson 1992; Usov 1992; Zhang & Mészáros 2001; Metzger et al. 2011; Rowlinson et al. 2014; Rea et al. 2015; Stratta et al. 2018; Fraija et al. 2021).

Using the magnetar scenario, Dainotti et al. (2013) and Dainotti et al. (2020b) showed that this relation can be seen in both X-ray and optical wavelengths with a slope of ≈ -1 . This relation in X-ray has been used to build a GRB Hubble diagram with redshift values up to $z > 8$ (Cardone et al. 2009, 2010; Postnikov et al. 2014; Dainotti et al. 2013). If this correlation also exists in radio, it could reveal information about the underlying GRB emission mechanisms and prove a step toward the standardization of the varied GRB population.

Our goal is to determine the existence of radio plateaus and examine the two-dimensional Dainotti correlation in radio. To our knowledge, this is the first such analysis with radio data, and thus the most complete multi-wavelength study of this relation. Our paper is organized as follows: in section 2, we describe our data sample. In section 3, we discuss the multi-wavelength Dainotti correlation, distribution of the isotropic energy in the prompt emission, E_{iso} and the rest frame time duration of the prompt emission T_{90}^* , and correlation between E_{iso} vs. the rest frame end time of the plateau emission, T_a^* and its correspondent luminosity, L_a , as well as a comparison of T_a^* in X-ray, optical, and radio. In section 4, we discuss the implications of the results achieved and present our conclusions.

2. DATA SELECTION

We take our sample from all published radio afterglows in the literature, mainly observed by the Very Large Array (VLA). The largest portion of our data comes from Chandra & Frail (2012), consisting of 304 radio afterglows observed from 1997 to 2011. We extend our search to 2020, gathering an additional 100 GRBs from the literature for a total sample of 404 GRBs. We also note that of this sample, four GRBs have been observed by NAOJ-affiliated telescopes - two by the Atacama Large Millimeter Array (ALMA), one by the Nobeyama 45-m Radio Telescope, and one by the East Asian VLBI Network (EAVN).

We then put our sample through a filtering process to obtain LCs useful for our analysis. We first reject all radio observations reporting only upper limits, bringing our sample to 211 GRBs. To attempt a fit to the radio LCs, we require at least five observations within the same frequency, discarding 127 GRBs that do not fit that criteria. We further discard 2 GRBs without known redshift, leaving us with a final sample of 82 GRBs.

Where the data is available, we consider multiple LCs within different frequency bands for one GRB. We therefore attempt to fit 202 LCs in total from our sample of 82 GRBs - on average, we fit LCs in 2-3 frequencies for each GRB, though some have more LCs (i.e. GRB030329, has 9 LCs.) We perform the fit with a broken power law (BPL) model, using the equation:

$$F(t) = \begin{cases} F_a \left(\frac{t}{T_a}\right)^{-\alpha_1} & t < T_a \\ F_a \left(\frac{t}{T_a}\right)^{-\alpha_2} & t \geq T_a, \end{cases} \quad (1)$$

¹ <https://www.mpe.mpg.de/~jcg/grbgen.html>

where F_a is the flux at the end of the plateau emission in $\text{erg cm}^{-2} \text{s}^{-1}$, T_a is the observed frame time in seconds at the end of the plateau emission, and α_1 and α_2 refer to the temporal power law decay indices before and after the break, respectively. The α_1 index is important because it determines the flatness of the plateau. We compute the flux in these units for ease of comparison to X-ray and optical data.

To compile our final sample, we first discard 75 LCs because the data of the LCs are too scattered to be fitted with a BPL. Then, we discard 18 LCs, because they do not support the shape of the BPL with a plateau (i.e. their $|\alpha_1| > 0.5$, or they can be fitted with a simple power law, etc.). In addition, 70 LCs don't fulfill the Avni (1978) prescription regarding the $\Delta\chi^2$ analysis, namely, we varied the $\Delta\chi^2$ so that the 1σ bounds could be determined assuming that the $\Delta\chi^2$ shape is a parabola for each of the parameters involved in the fitting, see Avni (1978) for additional details.

With this selection we are left with 39 LCs that display a clear break - however, we further reject 9 too steep to present a plateau, with $|\alpha_1| > 0.5$, and 12 from repeated GRBs. Thus, we find 18 LCs that resemble a plateau with $0 < |\alpha_1| < 0.5$. We report the best-fit parameters for the sample of 18 plateau GRBs in Table 1. All the errors quoted in this paper and gathered in Table 1 are calculated to 1σ . We show the LCs of the plateau sample in figure 1.

Of these 18 GRBs, all are classified as long GRBs, with (GRB 020903) classified as an X-ray flash (XRF), 1 (GRB 141121A) considered X-ray rich (XRR), and 2 with Supernova associations (Dainotti et al. 2017b). We classify GRBs with supernova associations according to the convention presented in Hjorth & Bloom (2012) in relation to the GRB-SNe Ic connection, with GRB030329 and GRB 980425 classified as “type-A” or SN-A, indicating strong spectroscopic evidence for the association.

We note that two GRBs, GRB 020903 and GRB 120326A, have very large error bars in the α_2 parameter - thus, we do not consider them in the subsequent analysis of the Dainotti correlation. However, we still include them in the plateau sample, as the sample size is small for the computation of the Efron & Petrosian method. In addition, those GRBs meet all other criteria for acceptance of the fit. A plot of α_2 vs. α_1 for the sample of 16 GRBs with a plateau used in the correlation analysis is shown in the left panel of figure 2. The same relation for the plateau sample plus the 9 additional GRBs with $|\alpha_1| > 0.5$, hereafter referred to as the “break” sample (as they can be reliably be fitted with a broken power law model, but the slope is too steep to be considered a plateau), is shown in the right panel of Fig. 2.

From the observed radio flux, we then compute the luminosity L_a at the time of break, T_a , using the equation:

$$L_a = 4\pi D_L^2(z) F_a(T_a) K, \quad (2)$$

where F_a is the observed flux at T_a , $D_L^2(z)$ is the luminosity distance assuming a flat Λ CDM model with $\Omega_M = 0.3$ and $H_0 = 70 \text{ km s}^{-1} \text{ Mpc}^{-1}$, and K is the k-correction:

$$K = \frac{1}{(1+z)^{\alpha_1 - \beta}}, \quad (3)$$

with β as the radio spectral index of the GRB (Chandra & Frail 2012). The β values were gathered from the literature; where no value existed, the average of the existing values, $\beta = 0.902$, was assigned, with the average of the known uncertainties $\sigma_\beta = 0.17$.

3. RESULTS

3.1. Luminosity-time correlation

For the LCs resembling a plateau, we examine the Dainotti correlation between L_a and the rest-frame time of break $T_a^* = \frac{T_a}{(1+z)}$ (the star * denotes the rest frame), similar to the work in Dainotti et al. (2017a) and Dainotti et al. (2020b) (figure 3). For a review on the afterglow correlations see Dainotti & Del Vecchio (2017); Dainotti & Amati (2018); Dainotti et al. (2018). We use the Bayesian D'Agostini method with the `cobaya` Python package to obtain our fitting parameters. Uncertainties are given to 1σ . The luminosity-time (Dainotti) correlation in radio is defined as:

$$\log L_{a,\text{radio}} = C_o + a_{\text{rad}} \times \log T_a^*, \quad (4)$$

where C_o is the normalization constant and a_{rad} is the slope determined by the linear fit. Using the sub-sample of 16 GRBs from the full plateau sample, we find best-fit parameters $C_o = 55.42 \pm 3.91$ and $a_{\text{rad}} = -2.34 \pm 0.66$. An ANOVA test gives a p-value that this correlation is drawn by chance of $p = 0.005$, and the Spearman ρ coefficient for this correlation is $\rho = -0.6$, indicating that the correlation is significant.

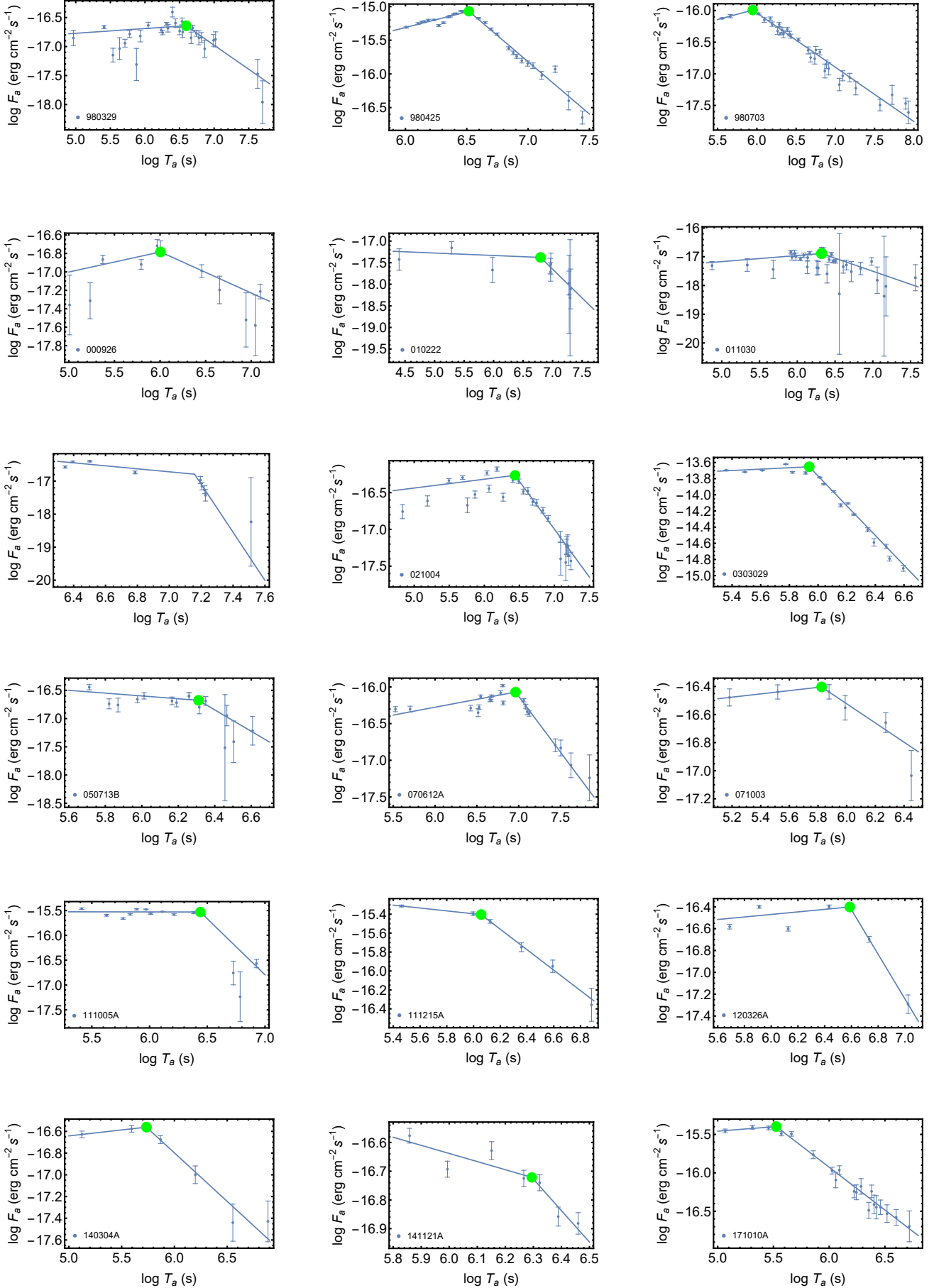


Figure 1. LCs accepted to plateau sample from BPL fitting.

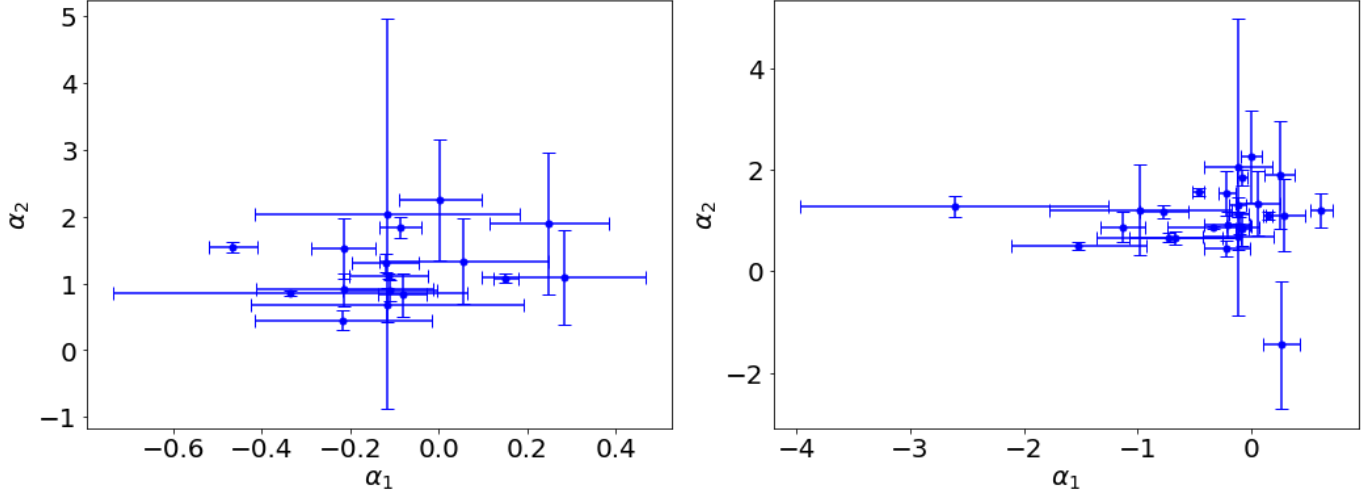


Figure 2. Left: α_2 vs. α_1 for “plateau” sample. Right: distribution for “plateau” sample plus the “break” sample.

We compare the results of the $L_a - T_a^*$ correlation in radio to the corresponding correlations in X-ray and optical (Dainotti et al. 2013, 2020b). We take our sample of 222 X-ray LCs from Dainotti et al. (2013), Dainotti et al. (2021a in preparation) and our sample of 131 optical LCs from Dainotti et al. (2020b), Dainotti et al. (2021b in preparation). To our knowledge, this is the first time such a comparison has been considered. We find a slope in X-ray of $a_X = -1.25 \pm 0.07$ and in optical of $a_{opt} = -0.97 \pm 0.07$. The radio slope agrees with these values within 2.1σ .

However, for a comparison that accounts for biases and redshift evolution, we apply the Efron-Petrosian (EP) method (Efron & Petrosian 1992) to recover their intrinsic slopes of the full sample of 18 plateau GRBs due to the paucity of the data (Dainotti et al. 2013, 2015b,a). To this end, we need to mimic the evolution of the variables with redshift with a simple function of redshift, $f(z) = (1+z)^\delta$, where δ is the slope of the evolutionary function determined by the EP method through the computation of a modified version of the Kendall τ statistics. The slope δ is found when $\tau = 0$, corresponding to the removal of the evolution. We update the analysis of the evolution in the X-ray sample (Dainotti et al. 2021a in preparation) and we find $T_a^{*'} = \frac{T_a^*}{(1+z)^{\delta T_a^*}}$ where $\delta T_a^* = -1.2 \pm 0.28$ and $L_a' = \frac{L_a}{(1+z)^{\delta L_a}}$ where $\delta L_a = 2.4 \pm 0.65$. For an updated optical sample (Dainotti et al. 2021b in preparation), we find $\delta T_a^* = -2.1 \pm 0.60$, which agrees with the X-ray value within 1.5σ , and $\delta L_a = 3.97 \pm 0.45$, which agrees within 2.4σ . This is more likely due to a difference in sample size than a result of an underlying physical process.

For the radio data, the luminosity limit has been determined using a method described in Dainotti et al. (2021b), in which a complete “parent” sample of GRBs with known peak fluxes are compared to a sub-sample of GRBs with known peak flux and known redshift. Here, the peak radio flux is defined as the highest flux observed in the LC, which coincides with T_a^* for the majority of the “break” sample. We therefore take the same convention for the parent sample.

The two-sample Kolmogorov-Smirnov (KS) test is then used to quantify the probability, as a function of flux limit, that the sub-sample is pulled from the parent sample. We find $> 90\%$ probability for all flux limits, with an observed increase in p-value beginning at $f_{lim} = -17.8$, in units of $\text{erg cm}^{-2} \text{s}^{-1}$, and reaching a plateau at 100% probability at $f_{lim} = -17.2$. Therefore, we choose -17.2 as the radio luminosity limit and find $\delta T_a^* = -1.94 \pm 0.86$, which agrees with the value in X-ray and optical within 1σ , and $\delta L_a = 3.15 \pm 1.65$, which also agrees within 1σ .

After applying the EP method using this prescription for limiting luminosity, we find the slope for the Dainotti correlation in radio as $a_{rad} = -0.26 \pm 0.71$. This is compatible with the corresponding correlation in X-ray, with a corrected slope of $a_X = -1.02 \pm 0.07$, within 1.07σ , and the corrected slope in optical, $a_{opt} = -0.79 \pm 0.06$, within 0.75σ . However, we note that two GRBs, GRB 980425 and GRB 111005A, appear to be outliers, with lower radio luminosity and redshift than the rest of the sample - if those GRBs are removed from the radio correlation, the slope of the corrected correlation becomes $a_{rad} = -0.45 \pm 0.47$. This value of the correlation, which we consider as the intrinsic value, has been corrected for the effects of selection bias and redshift evolution and does not consider systematically

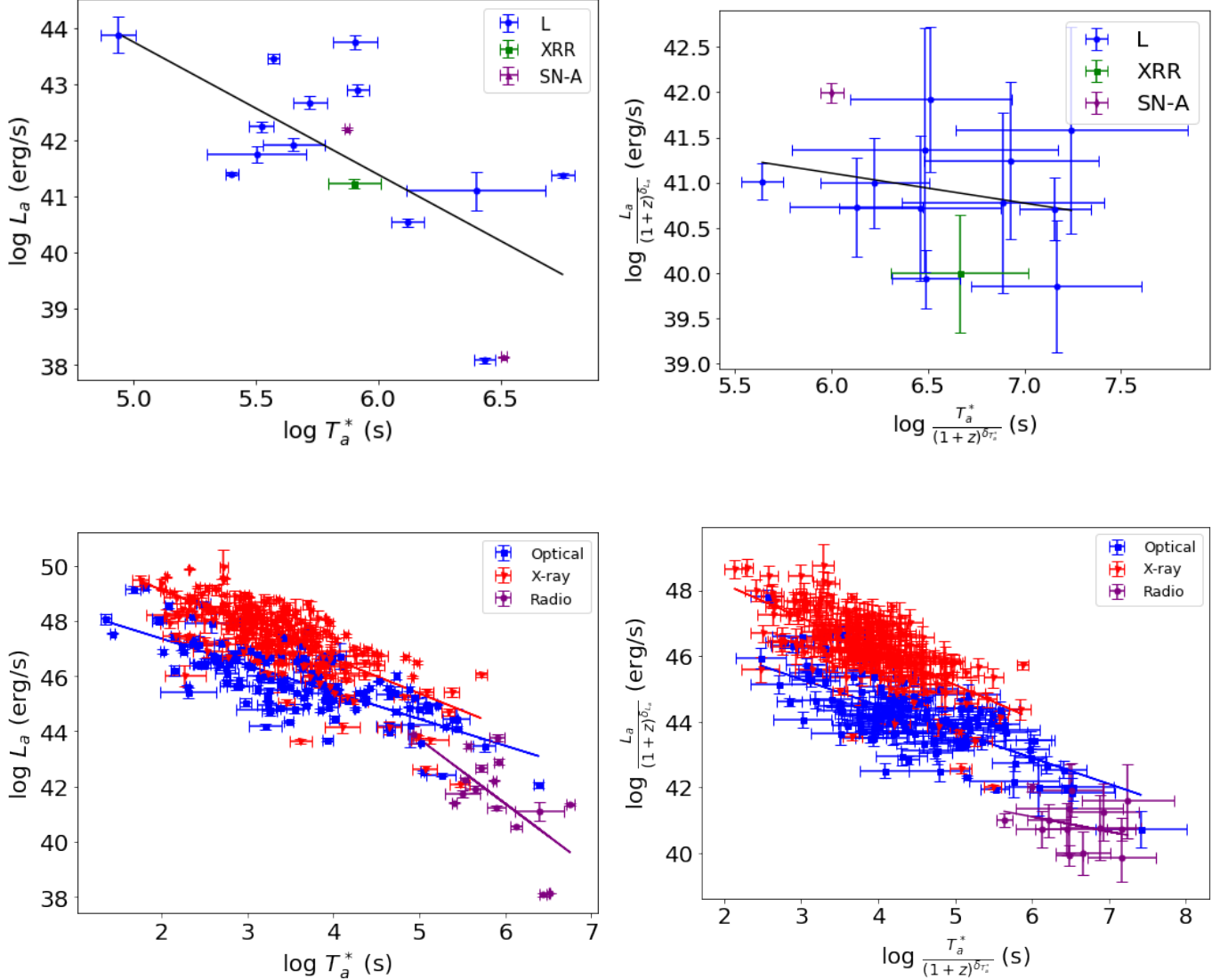


Figure 3. Top left: uncorrected $L_a - T_a^*$ correlation for 16 LCs, with GRBs differentiated by class: “L” refers to long GRBs, “XRR” corresponds to X-ray rich GRBs, and “SN-C” and “SN-A” correspond to type-A and type-C supernovae as described in section 2. Upper right: correlation corrected for selection biases, and with low-redshift outliers removed. Lower left: multi-wavelength $L_a - T_a^*$ correlation in X-ray, optical and radio shown in blue, red, and purple respectively. Lower right panel: correlation corrected for evolutionary effects with the same color code.

different, low-luminosity GRBs. This slope agrees with the slope of the corrected correlation in X-ray within 1.26σ and the corrected optical correlation within 0.72σ . We here stress that these two outliers are the closest GRBs at the smallest redshift - an order of magnitude less than the redshift of GRB 030329. It is highly likely that these two GRBs are off-axis GRBs and this is the reason why their luminosities are substantially lower than the ones expected at their specified redshift, for additional details see [Ryan et al. \(2015\)](#). The radio Dainotti correlation for the plateau sample is shown without the EP method corrections in the upper left panel of figure 3, and with the correction (and removal of outliers) in the upper right panel. The multi-wavelength correlations in X-rays, optical and radio, without corrections (left) and with corrections and removal of outliers (right), are shown in the lower panels. The X-ray, optical and radio data are shown in red, blue, and purple, respectively.

Looking at the distribution of radio data within the luminosity-time correlation by class (figure 3), we observe no particular clustering of any type of GRBs.

3.2. $E_{\text{iso}} - T_{90}^*$ distribution and the presence of LC breaks

To further investigate the behavior of the GRBs that present a break, we examine whether there is a relation between the existence of the break and the energy and duration of the prompt emission properties of a GRB. Thus, we investigate the distribution of the isotropic energy, E_{iso} vs. the rest-frame burst duration, $T_{90}^* = \frac{T_{90}}{(1+z)}$ for a subsample of 80 GRBs of the 82 GRBs considered for fitting, for which we could either find a value of E_{iso} in the literature or compute the value from the literature - where no value could be found (GRBs 050509C and 170105A), we compute the E_{iso} using the following equation:

$$E_{\text{iso}} = 4\pi D_L^2(z)SK, \quad (5)$$

where S is the fluence, $D_L^2(z)$ is defined as in equation (2), and K is the correction

$$K = \frac{1}{(1+z)^{1-\beta}}, \quad (6)$$

with β as the spectral index of the GRB. The S and β values are taken from the Swift/BAT GRB catalog ². We plot the distribution of the E_{iso} vs. T_{90}^* , shown in Figure 4. In the upper panels, we color-code the sample according to whether it presents a break - the blue refers to the 18 GRBs that present a break resembling a plateau, with $0 < |\alpha_1| < 0.5$; the red refers to the 9 GRBs that present a break, but with steeper $|\alpha_1| > 0.5$, and the grey refers to 53 GRBs that do not present a break. In the lower panels, we note from which satellite and instruments the GRBs have been observed: the Fermi Large Area Telescope (LAT), the Fermi Gamma Ray Burst Monitor (GBM), and Swift/BAT are shown in purple, blue, and cyan, respectively. The left panels show the GRB variables without the EP method correction, the right panels show the variables after correction for selection bias and redshift evolution.

Similar to the analysis performed for the Dainotti relation in radio shown in the previous section, we correct the $E_{\text{iso}} - T_{90}^*$ distribution for selection biases and redshift evolution using the EP method, which gives $E'_{\text{iso}} = \frac{E_{\text{iso}}}{(1+z)^{\delta_{E_{\text{iso}}}}}$ and $T'_{90} = \frac{T_{90}^*}{(1+z)^{\delta_{T_{90}^*}}}$ where $\delta_{E_{\text{iso}}} = 0.39 \pm 0.88$ and $\delta_{T_{90}^*} = -0.65 \pm 0.27$. The $\delta_{T_{90}^*}$ value agrees with values previously reported in Lloyd-Ronning et al. (2019, 2020) within 1σ , while the $\delta_{E_{\text{iso}}}$ agrees within 2.17σ . We show the corrected distribution in the lower two panels of figure 4, and find no particular trend or clustering after correction. An examination of the corrected T_{90}^* distribution alone (figure 6) shows overlap between the GRBs with a break and those without. A KS test between the two samples yields $KS = 0.18$ with $p = 0.56$, suggesting that they are drawn from the same parent sample.

3.3. Correlation of E_{iso} vs. L_a and T_a^*

To better understand the relation of the prompt emission to the radio afterglow, we further analyze the correlation of E_{iso} vs. L_a and E_{iso} vs. T_a^* , similar to the work done in Dainotti et al. (2011b) in X-rays. For the sample of 16 GRBs with a plateau considered for the $L_a - T_a^*$ correlation without correction, we find that the slope of the correlation between E_{iso} and T_a^* is -2.14 ± 0.96 , while the slope of the correlation between E_{iso} and L_a is 0.97 ± 0.17 . After correction for evolutionary effects and removal of the two low-luminosity GRBs, we find the slope after correction for E_{iso} vs. T_a^* is 0.23 ± 0.7 , while the slope for the corrected E_{iso} vs. L_a correlation is 0.61 ± 0.42 . This indicates that both correlations are susceptible to evolutionary effects - indeed, the correlation between E_{iso} vs. T_a^* nearly vanishes after correction, indicating that the original result is very likely a result of selection bias and redshift evolution. These results are shown in fig 5, with E_{iso} vs. T_a^* in the top panels and E_{iso} vs. L_a in the lower panels. The left panels show the uncorrected correlation, while the corrected correlation is shown in the right panels.

3.4. Comparison of T_a^* in X-ray, optical and radio

We compare the T_a^* distribution between the uncorrected and the corrected X-ray, optical, and radio samples to determine if the distributions are drawn from the same parent population (figure 6), similar to the work presented in Dainotti et al. (2020b). The X-ray sample of 222 GRBs presented in Dainotti et al. (2020a); Srinivasaragavan et al.

² https://swift.gsfc.nasa.gov/results/batgrbcatalog/index_tables.html

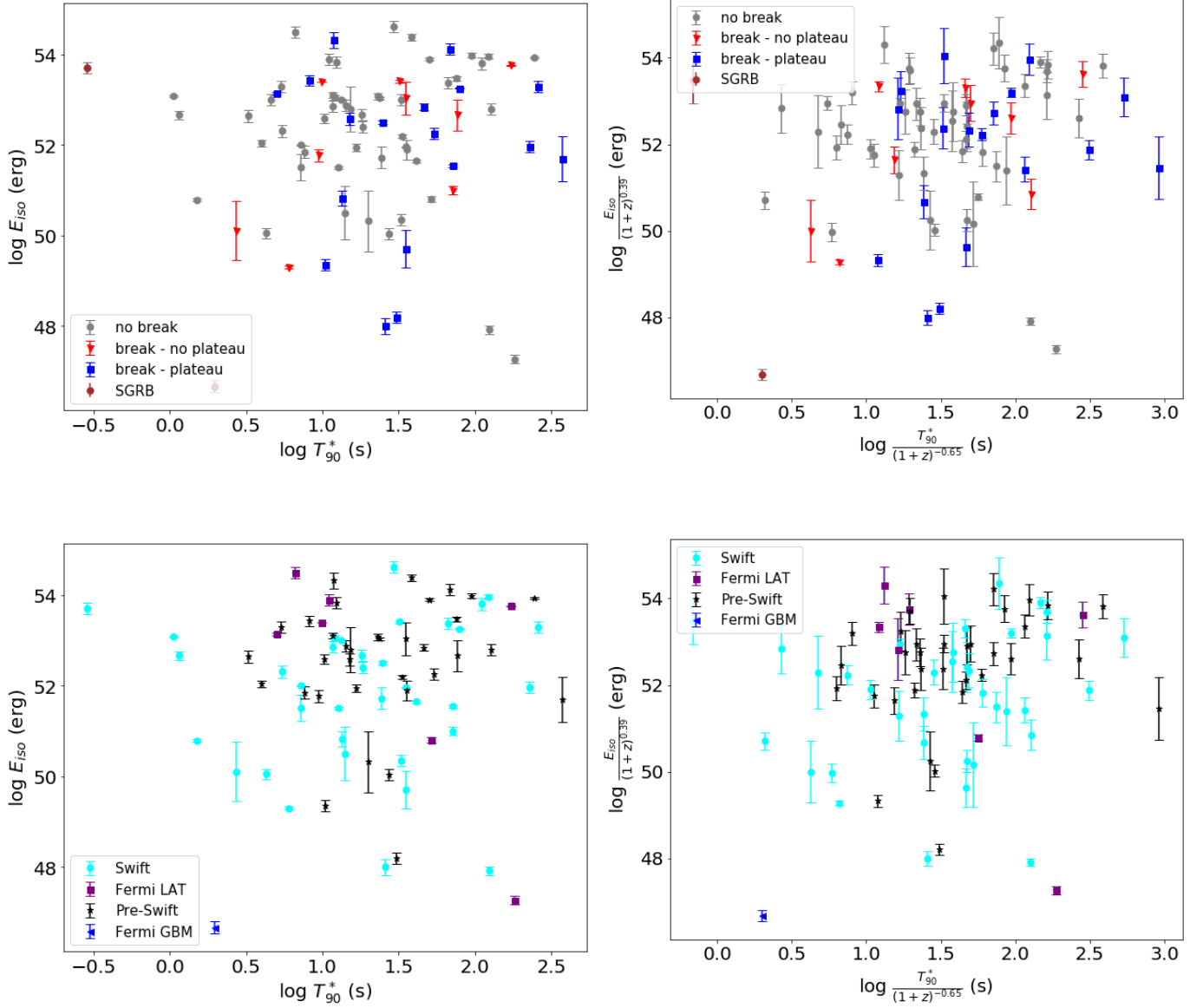


Figure 4. Left panel: $E_{\text{iso}} - T_{90}^*$ distribution color-coded according to whether the sample includes the break. Right panel: distribution color-coded by instrument. The lower left and right panel show the corrected distributions correspondent to the above panels.

(2020); Dainotti et al. (2021a) and the extended optical sample (131 GRBs vs 102 GRBs presented in Dainotti et al. (2020b)) show significant overlap, and a KS test between the two samples without correction gives a value of 0.16 with $p \approx 0.03$, while the comparison of the corrected samples gives a value of 0.31 with $p \approx 0$, indicating a slightly greater difference after correction. However, though both the X-ray and optical samples have an average T_a^* of $\sim 10^4$ seconds, the radio sample has a later average T_a^* of $\sim 10^6$ seconds. A KS test of the radio sample without correction vs. the X-ray and optical samples without correction produces a value of $KS = 0.96$ and $KS = 0.91$ with a p-value of ≈ 0 , respectively, while a comparison of the corrected samples produces a value of $KS = 0.99$ and $KS = 0.89$, respectively, with a p-value of ≈ 0 in both cases, indicating that in both the uncorrected and corrected samples the radio sample is significantly different. We discuss the possible physical mechanisms for this difference in section 4.

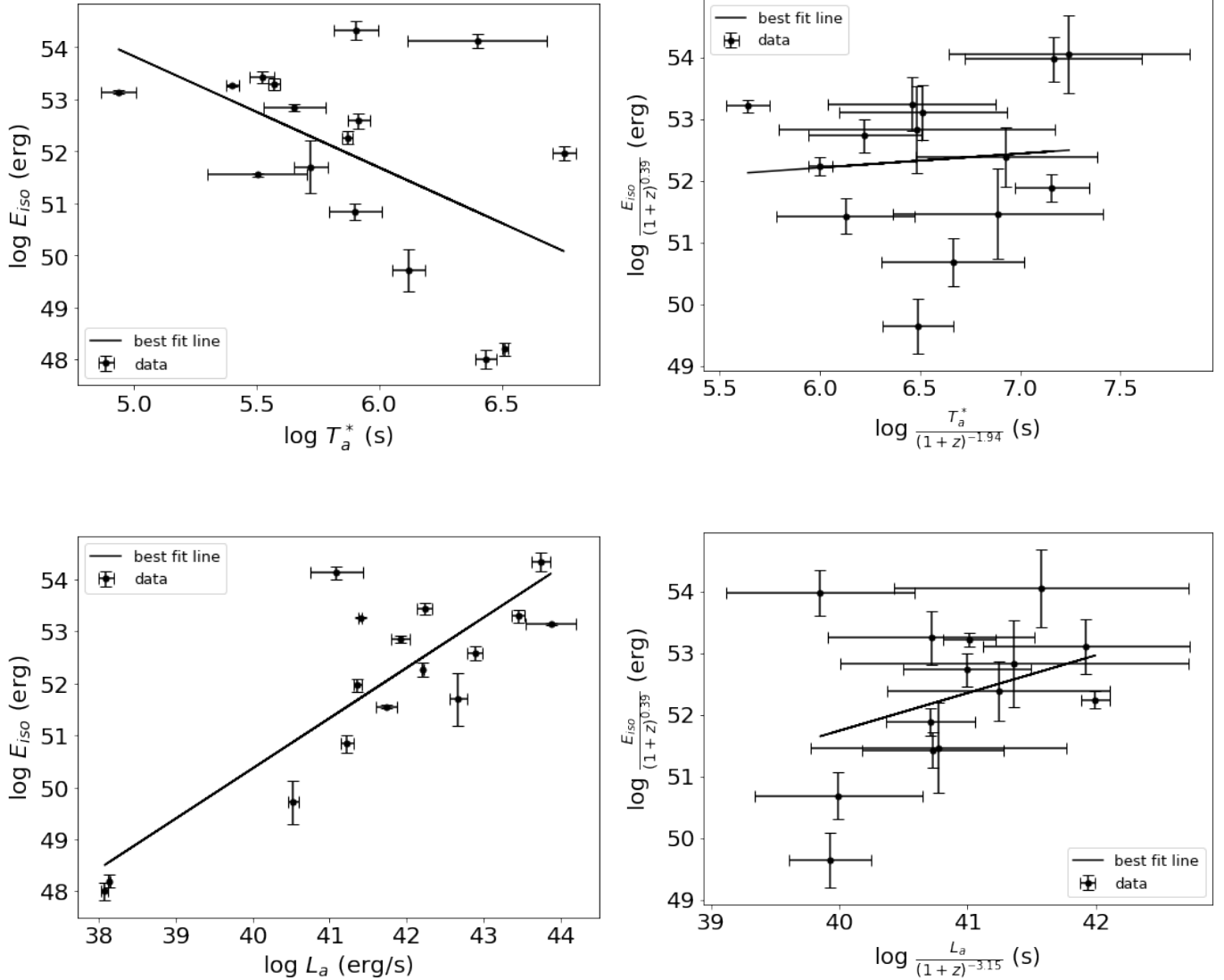


Figure 5. Top left: Uncorrected E_{iso} vs. T_a^* for sample of 16 GRBs with a plateau considered in section 3.1. Top right: E_{iso} vs. T_a^* after correction for evolutionary effects. Bottom panels: Uncorrected and corrected E_{iso} vs. L_a correlation for sample of 14 GRBs considered in the corrected Dainotti correlation, shown in left and right panels, respectively.

4. DISCUSSION AND CONCLUSIONS

Using the largest compilation of published GRB radio afterglows to date, we achieve two main findings : 1) 18 GRBs resemble a plateau feature in their LCs, and, 2) using this sample, the Dainotti correlation still holds for this radio sample, comparable within 2.1σ . After correction for evolutionary effects and removal of outliers, we find that the Dainotti radio correlation is compatible with the corresponding X-ray and optical correlations within 1.5σ , with a slope of $a_{\text{rad}} = -0.45 \pm 0.47$. As the slope of the corrected radio correlation agrees with -1 within 1.17σ , similar to the slope found in X-ray, this could indicate that the energy reservoir is conserved. One likely candidate for the production of the plateau is a black hole central engine, where the energy injection is driven by fall-back accretion onto the black hole. Kumar et al. (2008) suggests that the prompt emission is driven by accretion of the outer stellar

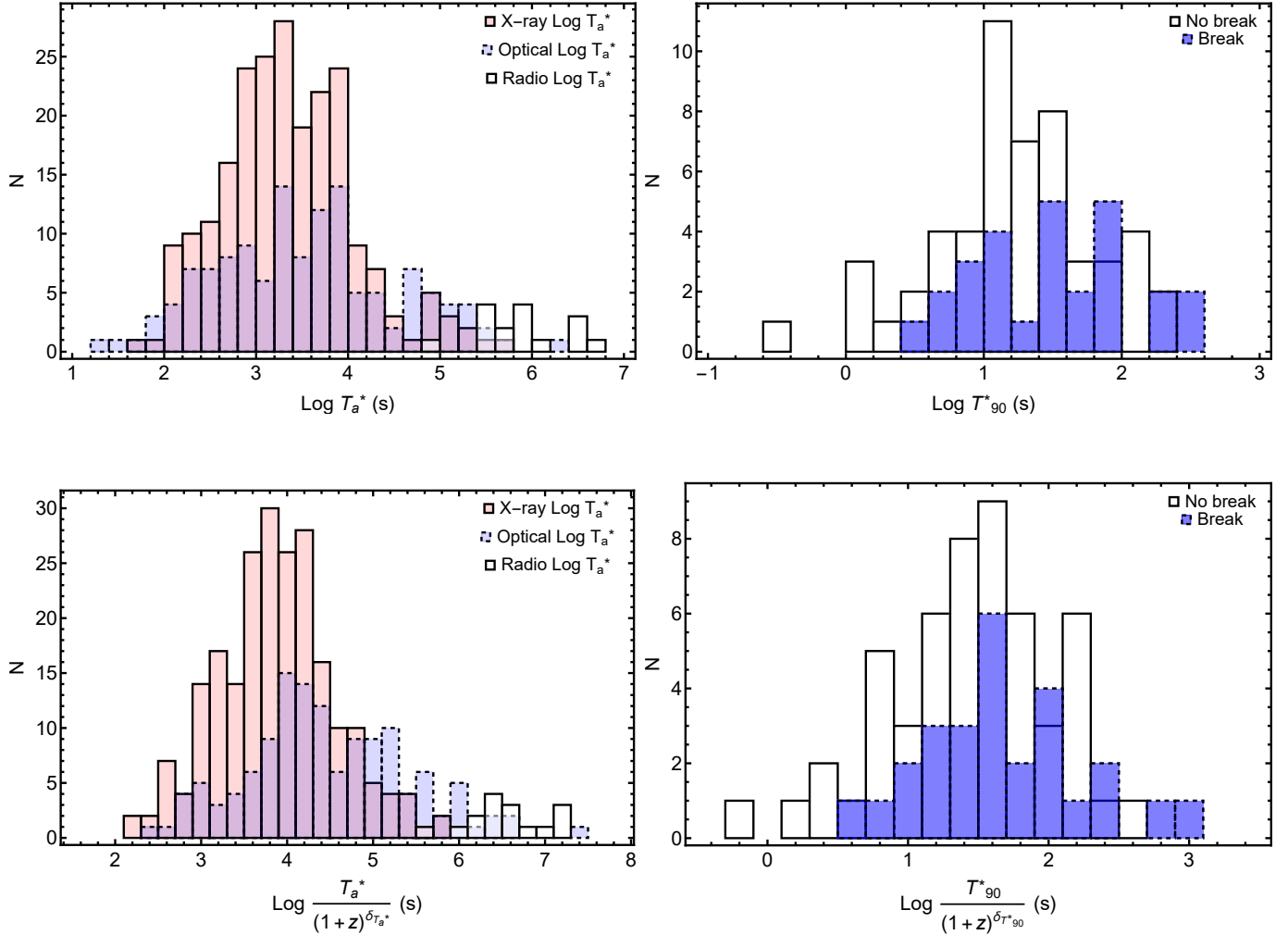


Figure 6. Left panels: Distribution of break time T_a^* for X-ray, optical, and radio samples. Right panels: T_{90}^* distribution for the sample of 80 GRBs, differentiated between GRBs with or without a break. Lower panels show the same distributions corrected for selection bias.

core, while the plateau phase seen in X-ray LCs is caused by the accretion of the stellar envelope of the progenitor, or is possibly driven by the magnetar.

Another important finding is that the radio break times occur significantly later than the other wavelengths. On average, the X-ray and optical plateaus last $\sim 10^4$ seconds, while radio plateaus last $\sim 10^6$ seconds. However, there are cases in which longer X-ray plateaus have been seen to last upwards of $\sim 10^5$ seconds, such as GRB 060218 and GRB 980425, detailed in [Dainotti et al. \(2017b\)](#). The late break times in radio could be a result of the peak of the spectrum appearing in the radio band at later times as the jet decelerates, consistent with the afterglow standard synchrotron shock model.

On the other hand, the late break could indicate that T_a^* is not the end of a plateau, but a break observed in radio wavelengths. The dynamics of the afterglow emission for an outflow propagating into surrounding constant-density medium has been widely explored ([Sari & Piran 1995](#); [Sari et al. 1996](#); [Sari 1997](#); [Sari et al. 1999](#)). The outflow transfers a large amount of its energy to this surrounding medium during the deceleration phase. Since the outflow launched into a cone of opening angle θ_j sweeps the surrounding medium, it decelerates, thus increasing the angular size of the emitting region ($\propto 1/\Gamma_j$). Once $1/\Gamma_j \approx \theta_j$, there will be no additional radiating elements from the jet if we assume a “top hat” jet, or another structure with a steep drop-off in energy per unit angle outside the core, producing a steepening in the LC. This “break” is expected to last from several hours to days (e.g., see [Kumar & Zhang 2015](#)).

Table 1. Sample of 18 GRBs that display a break and a plateau. Full sample of 82 GRBs used for fitting available online.

GRB	z	T_{90}	$\log F_a$ (erg/s cm^2)	$\log T_a$ (s)	α_1	α_2	$\log L_a$ (erg/s)	β	$\log E_{iso}$ (erg)	ref
980329	3.9	58	-16.64 ± 0.04	6.59 ± 0.09	-0.08 ± 0.06	0.83 ± 0.32	43.75 ± 0.12	1.7 ± 0.17	54.32 ± 0.18	[1]
980425	0.0085	31	-15.07 ± 0.01	6.52 ± 0.01	-0.46 ± 0.05	1.55 ± 0.08	38.14 ± 0.01	0.75 ± 0.17	48.20 ± 0.13	[1]
980703	0.966	90	-15.99 ± 0.11	5.95 ± 0.13	-0.33 ± 0.40	0.86 ± 0.03	41.92 ± 0.12	0.46 ± 0.2	52.84 ± 0.07	[1]
000926	2.039	25	-16.78 ± 0.05	6.01 ± 0.05	-0.22 ± 0.20	0.45 ± 0.15	42.24 ± 0.10	0.902 ± 0.17	53.43 ± 0.11	[1]
010222	1.477	170	-17.38 ± 0.33	6.80 ± 0.28	0.06 ± 0.19	1.33 ± 0.64	41.09 ± 0.34	0.902 ± 0.17	54.12 ± 0.13	[1]
011030	3	1500	-16.89 ± 0.05	6.32 ± 0.07	-0.21 ± 0.20	0.91 ± 0.25	42.67 ± 0.11	0.902 ± 0.17	51.69 ± 0.50	[1]
020903	0.25	13	-16.79 ± 0.29	7.16 ± 0.10	0.45 ± 0.38	7.29 ± 11.20	39.53 ± 0.29	0.902 ± 0.17	49.36 ± 0.12	[1]
021004	2.33	50	-16.27 ± 0.04	6.44 ± 0.04	-0.12 ± 0.08	1.30 ± 0.14	42.89 ± 0.10	0.9 ± 0.17	52.58 ± 0.14	[1]
030329	0.168	63	-13.65 ± 0.02	5.94 ± 0.02	-0.09 ± 0.05	1.84 ± 0.16	42.21 ± 0.02	-0.54 ± 0.02	52.26 ± 0.13	[1]
050713B	0.55	54.2	-16.68 ± 0.06	6.31 ± 0.07	0.25 ± 0.14	1.90 ± 1.05	40.53 ± 0.07	0.902 ± 0.17	49.71 ± 0.41	[1]
070612A	0.617	368.8	-16.07 ± 0.03	6.96 ± 0.05	-0.21 ± 0.07	1.52 ± 0.45	41.37 ± 0.05	0.902 ± 0.17	51.96 ± 0.13	[1]
071003	1.1	150	-16.40 ± 0.12	5.82 ± 0.20	-0.12 ± 0.31	0.68 ± 0.25	41.74 ± 0.14	0.902 ± 0.17	51.55 ± 0.03	[1]
111005A	0.0133	26	-15.53 ± 0.05	6.44 ± 0.04	0.00 ± 0.09	2.26 ± 0.90	38.08 ± 0.05	2.03 ± 0.27	48.00 ± 0.17	[2]
111215A	2.06	796	-15.40 ± 0.02	6.06 ± 0.02	0.15 ± 0.03	1.08 ± 0.08	43.45 ± 0.08	0.902 ± 0.17	53.29 ± 0.12	[3]
120326A	1.798	69.6	-16.40 ± 0.17	6.59 ± 0.27	-0.12 ± 0.30	2.04 ± 2.92	42.40 ± 0.19	0.902 ± 0.17	52.51 ± 0.04	[4]
140304A	5.283	31.2	-16.56 ± 0.04	5.73 ± 0.07	-0.11 ± 0.11	0.89 ± 0.16	43.88 ± 0.32	1.1 ± 0.4	53.14 ± 0.03	[5]
141121A	1.47	33.2	-16.72 ± 0.08	6.29 ± 0.11	0.28 ± 0.18	1.10 ± 0.71	41.23 ± 0.08	-0.18 ± 0.07	50.83 ± 0.16	[6]
171010A	0.3285	104	-15.40 ± 0.02	5.52 ± 0.03	-0.11 ± 0.09	1.11 ± 0.05	41.40 ± 0.02	1.9 ± 0.05	53.26 ± 0.01	[7]

NOTE—Note - Includes GRB ID, redshift, duration, best-fit parameters F_a , T_a^* , α_1 , α_2 , luminosity at time of break L_a , radio spectral index β , and E_{iso} . Redshift and T_{90} taken from Greiner (2021) and GCNs when not given in the literature. Best-fit parameters computed from BPL and reported as given by the fit, with the uncertainties at 1σ

L_a computed from best-fit parameters. β taken from the literature or set as the average. E_{iso} taken from the literature. References are as follows: [1] Chandra & Frail (2012), [2] Michalowski et al. (2018), [3] Zauderer et al. (2013), [4] Laskar et al. (2015), [5] Laskar et al. (2019), [6] Cucchiara et al. (2015), [7] Bright et al. (2019)

After this phase, the energy flux at radio bands is expected to evolve as $F_\nu \propto t^{-p}$ for $\nu_m < \nu < \nu_c$ and $\propto t^{-\frac{1}{3}}$ for $\nu < \nu_m < \nu_c$ (Sari et al. 1999). In our sample, the α_2 values, referring to an evolving slope of the decay phase, range from -0.27 to -0.9 with an average of -0.5, which could potentially support a decay within the $\nu < \nu_m < \nu_c$ regime.

Regarding whether the presence of the break is related to the prompt emission, we investigate the distribution between E_{iso} and T_{90}^* with and without correction for redshift evolution. We do not observe any trend or clustering in the sample of GRBs that present a break and those without, suggesting that E_{iso} and T_{90}^* are not indicators of a jet break within a radio LC. More analysis is needed to determine if there is another physical reason for this distinction.

In conclusion, we find:

1. After correction, the slope of the Dainotti correlation in radio agrees with the X-ray and optical within 1.5σ , instead of within 2.1σ when evolutionary effects are not considered. This emphasizes the importance of correcting for selection bias and that the two correlations can be interpreted within the same mechanism if we consider the slope of the correlation as a discriminant among models.
2. The time of break in the radio sample occurs later than in X-ray and optical, and the radio sample is found to be statistically different from the X-ray and optical samples. The late break time can be a result of the passage of the synchrotron characteristic break ($\nu_m \propto t^{-\frac{3}{2}}$) through radio wavelengths during the lateral expansion phase. After the break, the flux at radio bands is expected to evolve first as $F_\nu \propto t^{-\frac{1}{3}}$ for $\nu < \nu_m < \nu_c$ and later, as $\propto t^{-p}$ for $\nu_m < \nu < \nu_c$ (Sari et al. 1999). Another plausible explanation could be that the flux that dominates the radio bands is emitted in a wider decelerated shell (e.g., see Metzger & Bower 2014; Sironi & Giannios 2013; Fraija et al. 2021).
3. Analysis of the E_{iso} and T_{90}^* of 80 GRBs demonstrates that GRBs with and without a break in the LC appear to be drawn from the same parent population.

5. ACKNOWLEDGEMENTS

1 This work was made possible in part by the United States Department of Energy, Office of Science, Office of Workforce
 2 Development for Teachers and Scientists (WDTS) under the Science Undergraduate Laboratory Internships (SULI)
 3 program. We thank Dr. Cuellar for managing the SULI program at Stanford National Accelerator Laboratory. We
 4 also acknowledge the National Astronomical Observatory of Japan for their support in making this research possible,
 5 as well as Aleksander Lenart for helpful discussions during the writing of this paper. PC acknowledges support of the
 6 Department of Atomic Energy, Government of India, under project no. 12-R&D-TFR-1155 5.02-0700.

REFERENCES

- Avni, Y. 1978, *A&A*, 66, 307
- Bij de Vaate, J. G., de Villiers, D. I. L., Davidson, D. B., & van Cappellen, W. A. 2021, *Experimental Astronomy*, 51, 1, doi: [10.1007/s10686-020-09682-9](https://doi.org/10.1007/s10686-020-09682-9)
- Bright, J. S., Horesh, A., van der Horst, A. J., et al. 2019, *MNRAS*, 486, 2721, doi: [10.1093/mnras/stz1004](https://doi.org/10.1093/mnras/stz1004)
- Cardone, V. F., Capozziello, S., & Dainotti, M. G. 2009, *MNRAS*, 400, 775, doi: [10.1111/j.1365-2966.2009.15456.x](https://doi.org/10.1111/j.1365-2966.2009.15456.x)
- Cardone, V. F., Dainotti, M. G., Capozziello, S., & Willingale, R. 2010, *MNRAS*, 408, 1181, doi: [10.1111/j.1365-2966.2010.17197.x](https://doi.org/10.1111/j.1365-2966.2010.17197.x)
- Chandra, P., & Frail, D. A. 2012, *ApJ*, 746, 156, doi: [10.1088/0004-637X/746/2/156](https://doi.org/10.1088/0004-637X/746/2/156)
- Cucchiara, A., Veres, P., Corsi, A., et al. 2015, *ApJ*, 812, 122, doi: [10.1088/0004-637X/812/2/122](https://doi.org/10.1088/0004-637X/812/2/122)
- Dainotti, M., Petrosian, V., Willingale, R., et al. 2015a, *MNRAS*, 451, 3898, doi: [10.1093/mnras/stv1229](https://doi.org/10.1093/mnras/stv1229)
- Dainotti, M. G., & Amati, L. 2018, *PASP*, 130, 051001, doi: [10.1088/1538-3873/aaa8d7](https://doi.org/10.1088/1538-3873/aaa8d7)
- Dainotti, M. G., Cardone, V. F., & Capozziello, S. 2008, *MNRAS*, 391, L79, doi: [10.1111/j.1745-3933.2008.00560.x](https://doi.org/10.1111/j.1745-3933.2008.00560.x)
- Dainotti, M. G., & Del Vecchio, R. 2017, *NewAR*, 77, 23, doi: [10.1016/j.newar.2017.04.001](https://doi.org/10.1016/j.newar.2017.04.001)
- Dainotti, M. G., Del Vecchio, R., Shigehiro, N., & Capozziello, S. 2015b, *ApJ*, 800, 31, doi: [10.1088/0004-637X/800/1/31](https://doi.org/10.1088/0004-637X/800/1/31)
- Dainotti, M. G., Del Vecchio, R., & Tarnopolski, M. 2018, *Advances in Astronomy*, 2018, 4969503, doi: [10.1155/2018/4969503](https://doi.org/10.1155/2018/4969503)
- Dainotti, M. G., Fabrizio Cardone, V., Capozziello, S., Ostrowski, M., & Willingale, R. 2011a, *ApJ*, 730, 135, doi: [10.1088/0004-637X/730/2/135](https://doi.org/10.1088/0004-637X/730/2/135)
- Dainotti, M. G., Hernandez, X., Postnikov, S., et al. 2017a, *ApJ*, 848, 88, doi: [10.3847/1538-4357/aa8a6b](https://doi.org/10.3847/1538-4357/aa8a6b)
- Dainotti, M. G., Lenart, A. L., Fraija, N., et al. 2021a, *PASJ*, 73, 970, doi: [10.1093/pasj/psab057](https://doi.org/10.1093/pasj/psab057)
- Dainotti, M. G., Lenart, A. L., Sarracino, G., et al. 2020a, *ApJ*, 904, 97, doi: [10.3847/1538-4357/abbe8a](https://doi.org/10.3847/1538-4357/abbe8a)
- Dainotti, M. G., Nagataki, S., Maeda, K., Postnikov, S., & Pian, E. 2017b, *A&A*, 600, A98, doi: [10.1051/0004-6361/201628384](https://doi.org/10.1051/0004-6361/201628384)
- Dainotti, M. G., Ostrowski, M., & Willingale, R. 2011b, *MNRAS*, 418, 2202, doi: [10.1111/j.1365-2966.2011.19433.x](https://doi.org/10.1111/j.1365-2966.2011.19433.x)
- Dainotti, M. G., Petrosian, V., & Bowden, L. 2021b, *ApJL*, 914, L40, doi: [10.3847/2041-8213/abf5e4](https://doi.org/10.3847/2041-8213/abf5e4)
- Dainotti, M. G., Petrosian, V., Singal, J., & Ostrowski, M. 2013, *ApJ*, 774, 157, doi: [10.1088/0004-637X/774/2/157](https://doi.org/10.1088/0004-637X/774/2/157)
- Dainotti, M. G., Postnikov, S., Hernandez, X., & Ostrowski, M. 2016, *ApJL*, 825, L20, doi: [10.3847/2041-8205/825/2/L20](https://doi.org/10.3847/2041-8205/825/2/L20)
- Dainotti, M. G., Livermore, S., Kann, D. A., et al. 2020b, *ApJL*, 905, L26, doi: [10.3847/2041-8213/abcda9](https://doi.org/10.3847/2041-8213/abcda9)
- Duncan, R. C., & Thompson, C. 1992, *ApJL*, 392, L9, doi: [10.1086/186413](https://doi.org/10.1086/186413)
- Efron, B., & Petrosian, V. 1992, *ApJ*, 399, 345, doi: [10.1086/171931](https://doi.org/10.1086/171931)
- Fraija, N., Kamenetskaia, B. B., Dainotti, M. G., et al. 2021, *ApJ*, 907, 78, doi: [10.3847/1538-4357/abcaf6](https://doi.org/10.3847/1538-4357/abcaf6)
- Fraija, N., Laskar, T., Dichiaro, S., et al. 2020a, *ApJ*, 905, 112, doi: [10.3847/1538-4357/abc41a](https://doi.org/10.3847/1538-4357/abc41a)
- Fraija, N., Veres, P., Beniamini, P., et al. 2020b, arXiv e-prints, arXiv:2003.11252, <https://arxiv.org/abs/2003.11252>
- Hjorth, J., & Bloom, J. S. 2012, *The Gamma-Ray Burst - Supernova Connection*, 169–190
- Johnston, S., Bailes, M., Bartel, N., et al. 2007, *PASA*, 24, 174, doi: [10.1071/AS07033](https://doi.org/10.1071/AS07033)
- Kumar, P., Narayan, R., & Johnson, J. L. 2008, *Science*, 321, 376, doi: [10.1126/science.1159003](https://doi.org/10.1126/science.1159003)
- Kumar, P., & Zhang, B. 2015, *PhR*, 561, 1, doi: [10.1016/j.physrep.2014.09.008](https://doi.org/10.1016/j.physrep.2014.09.008)
- Laskar, T., Berger, E., Margutti, R., et al. 2015, *ApJ*, 814, 1, doi: [10.1088/0004-637X/814/1/1](https://doi.org/10.1088/0004-637X/814/1/1)
- Laskar, T., van Eerten, H., Schady, P., et al. 2019, *ApJ*, 884, 121, doi: [10.3847/1538-4357/ab40ce](https://doi.org/10.3847/1538-4357/ab40ce)
- Liang, E.-W., Zhang, B.-B., & Zhang, B. 2007, *ApJ*, 670, 565, doi: [10.1086/521870](https://doi.org/10.1086/521870)

- Lloyd-Ronning, N., Hurtado, V. U., Aykotalp, A., Johnson, J., & Ceccobello, C. 2020, MNRAS, 494, 4371, doi: [10.1093/mnras/staa1057](https://doi.org/10.1093/mnras/staa1057)
- Lloyd-Ronning, N. M., Aykotalp, A., & Johnson, J. L. 2019, MNRAS, 488, 5823, doi: [10.1093/mnras/stz2155](https://doi.org/10.1093/mnras/stz2155)
- Metzger, B. D., & Bower, G. C. 2014, MNRAS, 437, 1821, doi: [10.1093/mnras/stt2010](https://doi.org/10.1093/mnras/stt2010)
- Metzger, B. D., Giannios, D., Thompson, T. A., Bucciantini, N., & Quataert, E. 2011, MNRAS, 413, 2031, doi: [10.1111/j.1365-2966.2011.18280.x](https://doi.org/10.1111/j.1365-2966.2011.18280.x)
- Oates, S. R., Page, M. J., De Pasquale, M., et al. 2012, MNRAS, 426, L86, doi: [10.1111/j.1745-3933.2012.01331.x](https://doi.org/10.1111/j.1745-3933.2012.01331.x)
- Postnikov, S., Dainotti, M. G., Hernandez, X., & Capozziello, S. 2014, ApJ, 783, 126, doi: [10.1088/0004-637X/783/2/126](https://doi.org/10.1088/0004-637X/783/2/126)
- Rea, N., Gullón, M., Pons, J. A., et al. 2015, ApJ, 813, 92, doi: [10.1088/0004-637X/813/2/92](https://doi.org/10.1088/0004-637X/813/2/92)
- Rowlinson, A., Gompertz, B. P., Dainotti, M., et al. 2014, MNRAS, 443, 1779, doi: [10.1093/mnras/stu1277](https://doi.org/10.1093/mnras/stu1277)
- Ryan, G., van Eerten, H., MacFadyen, A., & Zhang, B.-B. 2015, ApJ, 799, 3, doi: [10.1088/0004-637X/799/1/3](https://doi.org/10.1088/0004-637X/799/1/3)
- Sakamoto, T., Hill, J. E., Yamazaki, R., et al. 2007, ApJ, 669, 1115, doi: [10.1086/521640](https://doi.org/10.1086/521640)
- Sari, R. 1997, ApJL, 489, L37, doi: [10.1086/310957](https://doi.org/10.1086/310957)
- Sari, R., Narayan, R., & Piran, T. 1996, ApJ, 473, 204, doi: [10.1086/178136](https://doi.org/10.1086/178136)
- Sari, R., & Piran, T. 1995, ApJL, 455, L143, doi: [10.1086/309835](https://doi.org/10.1086/309835)
- Sari, R., Piran, T., & Halpern, J. P. 1999, ApJL, 519, L17, doi: [10.1086/312109](https://doi.org/10.1086/312109)
- Schinckel, A. E., Bunton, J. D., Chippendale, A. P., et al. 2011, in Microwave Conference Proceedings (APMC), 1178
- Sironi, L., & Giannios, D. 2013, ApJ, 778, 107, doi: [10.1088/0004-637X/778/2/107](https://doi.org/10.1088/0004-637X/778/2/107)
- Srinivasaragavan, G. P., Dainotti, M. G., Fraija, N., et al. 2020, ApJ, 903, 18, doi: [10.3847/1538-4357/abb702](https://doi.org/10.3847/1538-4357/abb702)
- Stratta, G., Dainotti, M. G., Dall’Osso, S., Hernandez, X., & De Cesare, G. 2018, ApJ, 869, 155, doi: [10.3847/1538-4357/aadd8f](https://doi.org/10.3847/1538-4357/aadd8f)
- Thompson, C., & Duncan, R. C. 1993, ApJ, 408, 194, doi: [10.1086/172580](https://doi.org/10.1086/172580)
- Usov, V. V. 1992, Nature, 357, 472, doi: [10.1038/357472a0](https://doi.org/10.1038/357472a0)
- Zauderer, B. A., Berger, E., Margutti, R., et al. 2013, ApJ, 767, 161, doi: [10.1088/0004-637X/767/2/161](https://doi.org/10.1088/0004-637X/767/2/161)
- Zhang, B., & Mészáros, P. 2001, ApJL, 552, L35, doi: [10.1086/320255](https://doi.org/10.1086/320255)
- Zhang, B., Zhang, B.-B., Virgili, F. J., et al. 2009, ApJ, 703, 1696, doi: [10.1088/0004-637X/703/2/1696](https://doi.org/10.1088/0004-637X/703/2/1696)